Available online at www.sciencedirect.com

SciVerse ScienceDirect

Ceramics International 39 (2013) 6945–6952

CERAMICS INTERNATIONAL

www.elsevier.com/locate/ceramint

Preparation, microstructure and magnetic properties of Fe-containing SiC ceramic nanocomposites derived from $Fe(CO)_5$-modified AHPCS

Zhaoju Yu*, Junying Zhan, Zehui Zhang, Le Yang

College of Materials, Key Laboratory of High Performance Ceramic Fibers (Xiamen University), Ministry of Education, Xiamen 361005, China

Received 7 January 2013; received in revised form 22 January 2013; accepted 13 February 2013
Available online 19 February 2013

Abstract

Fe-containing SiC ceramic nanocomposites were prepared by pyrolysis of iron pentacarbonyl ($Fe(CO)_5$)-modified allylhydridopolycarbosilane (AHPCS-$Fe(CO)_5$). The cross-linking mechanism and ceramization of the AHPCS-$Fe(CO)_5$ precursors were studied by nuclear magnetic resonance, Fourier transform infrared spectroscopy and thermal gravimetric analysis. It is suggested that hydrosilylation, dehydrocoupling and the reaction of Si–H bonds with C═O groups evolved by $Fe(CO)_5$ decomposition are involved in the cross-linking of the AHPCS-$Fe(CO)_5$ precursor. The crystallization behavior, microstructure and magnetic properties of the obtained Fe-containing SiC ceramic nanocomposites were investigated by techniques such as X-ray diffraction, scanning electron microscopy, transmission electron microscopy and vibrating sample magnetometry. The results indicate that the α-Fe crystallites together with β-SiC crystallites and poorly organized turbostratic carbon are dispersed in an amorphous SiC_xO_y matrix, which might be responsible for the soft magnetization of the obtained ceramic composites. The iron content and the magnetic properties of the final ceramic could be easily tuned by the amount of $Fe(CO)_5$ in the precursor.

Keywords: Polymer-derived ceramics; Silicon carbide; Ceramic nanocomposites; Magnetic ceramics

1. Introduction

High-performance ceramics, especially Si-based materials, are of considerable interest because of their high thermal and chemical stability, low density, high mechanical strength and hardness [1–5]. Recently, some researchers have paid more attention to the electrical and magnetic properties of Si-based ceramics [6–15].

It is well known that iron has the highest magnetic moment among all 3d transition metals. The incorporation of iron into Si-based ceramics is desirable as it will introduce interesting magnetic properties. Literature search indicates that only a few investigations [6,16–19] have been carried out to prepare iron-containing SiC ceramics using the polymer-derived ceramic (PDC) route. Maclachlan et al. [6] prepared a shaped magnetic ceramic by the pyrolysis of poly (ferrocenylsilanes) precursors. The magnetic properties of the shaped ceramic could be tuned between superparamagnetic and ferromagnetic by adjusting the pyrolysis conditions. Sun et al. [16,17] synthesized a series of hyperbranched poly[ferrocenylene(methyl)silyne] polymers to prepare mesoporous, conductive, and magnetic FeSiC ceramics. Chen et al. [18] synthesized a new polyferrocarbosilane from polydimethylsilane and ferrocene, which exhibits good spinnability and has been converted to magnetic Si–Fe–C–O fibers by high temperature pyrolysis in an inert atmosphere. However, those works involve a relatively complicated synthetic route during the preparation of iron-containing polymeric precursor. More recently, Chen et al. [19] prepared iron nanoparticle-containing SiC fibers by using an iron-containing polycarbosilane (Fe-PCS) as precursor. Iron pentacarbonyl ($Fe(CO)_5$) first reacted with low-molecular-weight polycarbosilane (PCS) to form an iron-containing colloid. The colloid was then added into high-molecular-weight PCS to form Fe-PCS, which led to magnetic SiC fibers after pyrolysis.

In the past two decades, a liquid hyperbranched PCS (HBPCS) has been regarded as an excellent effective

*Corresponding author. Tel.: +86 133 287 80080.
E-mail address: zhaojuyu@xmu.edu.cn (Z. Yu).

0272-8842/$ - see front matter
http://dx.doi.org/10.1016/j.ceramint.2013.02.031

precursor especially for a matrix source because of its unique structures and favorable properties [20,21]. In our previous work, a series of HBPCSs such as allylhydridopolycarbosilane (AHPCS), ethynylhydridopolycarbosilane and propargylhydridopolycarbosilane were synthesized [22–25]. An important consideration is the ceramic yield when choosing a ceramic precursor. It is well accepted that cross-linking of preceramic polymers is a prevalent method for increasing the ceramic yield because it reduces the amount of volatile decomposition products [6]. In this regard, we tended to explore an efficient cross-linking agent in order to lower the cross-linking temperature while improving the ceramic yield of this type of HBPCS [26–29].

In this paper, we tried to use $Fe(CO)_5$ as a cross-linking agent to improve the cross-linking of AHPCS as well as acts as a new source of Fe for the final ceramic nanocomposites. It is interesting to point out that $Fe(CO)_5$ is also an important catalyst for hydrosilylation (a reaction between Si–H and C=C groups) [30,31]. Therefore, we expected that $Fe(CO)_5$ could efficiently catalyze the hydrosilylation of AHPCS, which contains a large amount of C=C groups and Si–H_x groups. The detailed cross-linking mechanism of the AHPCS-$Fe(CO)_5$ precursor was studied, and the in situ synthesis of the SiFeC nanocomposites by the PDC route was investigated. The structural evolution during the ceramization process, microstructure and magnetic properties of the final ceramics were also studied.

2. Experimental sections

2.1. Materials

All manipulations were carried out using standard high-vacuum or insert-atmosphere techniques as described by Shriver and Drezdzon [32]. AHPCS with a composition formula $[SiH_{1.26}(CH_3)_{0.60}(CH_2CH=CH_2)_{0.14}CH_2]_n$ was prepared, as previously described [23], by a one-pot synthesis with $Cl_2Si(CH_3)CH_2Cl$, Cl_3SiCH_2Cl, and $CH_2=CHCH_2Cl$ as the starting materials. The AHPCS used in this work had a number-average molecular weight of ca. 700 and a polydispersity index of 1.96. Iron pentacarbonyl [$Fe(CO)_5$, 99%] was provided by Tian-Yi Submicron Metal Co., Ltd. (Jiang Su, China). Other commercially available reagents were used as received.

2.2. Cross-linking

Preparation and cross-linking of AHPCS–$Fe(CO)_5$ precursors, abbreviated as AF, were carried out in a Schlenk flask with a reflux condenser, a magnetic stirrer and an argon inlet. Certain amount of $Fe(CO)_5$ was introduced into the Schlenk flask in an argon atmosphere, and then liquid AHPCS was added to dissolve $Fe(CO)_5$ until a clear solution was obtained. The weight ratios of $Fe(CO)_5$ to AHPCS were 1/6, 1/3 and 2/3, and were abbreviated as AF-1, AF-2 and AF-3, correspondingly. Finally, the Schlenk flask was heated in a 150 °C oil bath. The AF solution solidified immediately into a compact, light brown, rubbery solid and was kept at this temperature for 6 h. A control test was performed under the same conditions but no $Fe(CO)_5$ was added. These cross-linked AFs and AHPCS were used both for TGA and for macroscopic pyrolysis.

2.3. Pyrolysis

With the pyrolysis temperature (Tp) of 900 °C, the cross-linked sample was put in an aluminum boat and heated in a glass silica tube under an argon flow. The temperature was progressively raised up to Tp at a rate of 5 °C/min and kept at this value for 2 h. For Tp > 900 °C, the sample (pre-pyrolysed at 900 °C) was put in a graphite crucible and heated in a tube furnace in argon. The pre-pyrolysed sample was heated rapidly to Tp at a rate of 40 °C min^{-1} and kept at this temperature for 2 h. After pyrolysis, the resulting ceramics were furnace-cooled to room temperature (RT).

2.4. Characterization

Fourier transform infrared spectroscopy (FT IR) spectra were recorded on a Nicolet Avator 360 apparatus (Nicolet, Madison, WI) with KBr plates for liquid samples and KBr discs for solid samples. Nuclear magnetic resonance (NMR) experiments were carried out on a Bruker AV 300 MHz spectrometer (Bruker, Germany) operating at 75.46 MHz for carbon-13 (^{1}H-decoupling). The specimen used for ^{13}C NMR was dissolved in $CDCl_3$ solution. The ^{13}C chemical shifts were referred to tetramethylsilane (TMS) (assigned to 0 ppm). The solid-state ^{13}C magic angle spinning (MAS) NMR experiments were also performed on a Bruker AV 300 NMR spectrometer using a 4.0 mm Bruker double resonance MAS probe. The samples were spun at 5.0 kHz. The ^{13}C isotropic chemical shifts were referenced to the carbonyl carbon of glycine (assigned to 173.2 ppm). Thermal analysis of the samples was performed by thermal gravimetric analysis (TGA) (Netzsch STA 409C, Netzsch, Germany) in argon gas with a heating rate of 10 °C/min ranging from RT to 1200 °C. X-ray diffraction (XRD) studies were executed on a PANalytical X'Pert PRO diffractometer (PANalytical, Netherlands) with Cu K_α radiation. The specimens were continuously scanned from 10° to 90° (2θ) at a speed of 0.0167° s^{-1}. The elemental analysis of the ceramics was performed by an energy dispersive spectrometer (EDS, JEOL, Japan). The morphologies of the ceramics were examined with a scanning electron microscope (SEM) (Model 1530, LEO, Germany). Transmission electron microscopy (TEM) observations and high resolution imaging were performed using a JEM 2100 (JEOL, Japan) operated at 200 kV. The magnetic properties of the ceramics were measured using a vibrating sample magnetometry system (TOEIVSM-5-15, Japan) at RT with a

standard sample of Ni, and then Hk was determined by calculating the measured easy axis and hard axis loops of the reduced magnetization.

(1)

3. Results and discussion

3.1. Cross-linking

According to the literature [19], $Fe(CO)_5$ did react with low-molecular-weight PCS which was prepared by Yajima's route. It was found that $Fe(CO)_5$ first decomposed under heat into nanosized carbonyl derivatives and CO. CO then reacted with PCS at the interface, rendering the PCS cross-linked [19]. In comparison with the Yajima PCS, the AHPCS has more reactive C=C bonds and Si–H bonds such as SiH, SiH_2 and SiH_3 units [22,23]. Based on this fact, the cross-linking of the AHPCS would be improved by the introduction of $Fe(CO)_5$.

The cross-linking of AHPCS-$Fe(CO)_5$ precursors was investigated by NMR and FT IR. As the polymers became insoluble upon cross-linking at intermediate temperatures, solid-state NMR was the available way to study the chemical structural changes. Fig. 1 shows ^{13}C NMR spectrum of the soluble AHPCS and solid-state ^{13}C MAS NMR spectra of the cross-linked AHPCS-$Fe(CO)_5$ precursors.

The weight ratios of $Fe(CO)_5$ to AHPCS are 1/6, 1/3 and 2/3, and the resultant samples are abbreviated as AF-1, AF-2 and AF-3, correspondingly. For the cross-linked AHPCS, the intensity of carbon signals of C=C groups (114 and 135 ppm) decreases in comparison with that of the original AHPCS, indicating that C=C groups are involved in the cross-linking. According to our previous study [29–31], the consumption of C=C groups is due to the hydrosilylation of the AHPCS (Eq. (1)). For the cross-linked AHPCS-$Fe(CO)_5$ precursors, carbon signals of C=C groups at 114 and 135 ppm almost disappear, indicating that the hydrosilylation of AHPCS is obviously improved by the introduction of $Fe(CO)_5$.

The cross-linking reaction of AHPCS–$Fe(CO)_5$ precursors was further investigated by FT IR (Fig. 2). From a comparison of the FT IR spectra of the cross-linked AF precursors with those of AHPCS and $Fe(CO)_5$, it is observed that the AF spectra contain characteristic peaks of AHPCS and $Fe(CO)_5$. Careful examination indicates that the peaks at 3077 cm^{-1} (C–H stretch in –CH=CH_2) in the AFs almost disappear in comparison with those in the original AHPCS and cross-linked AHPCS. The FT IR results agree well with the NMR, supporting once again the fact that the hydrosilylation could be significantly improved by $Fe(CO)_5$.

Moreover, the peak at 2140 cm^{-1} (Si–H stretch) of the AFs obviously decreases, compared with those of the original AHPCS and the cross-linked AHPCS. Herein, the intensity ratio of the peak at 2140 cm^{-1} (Si–H) to that at 1250 cm^{-1} (Si–CH_3), indicating the Si–H content, is denoted as A(Si–H)/A(Si–CH_3). As shown in Fig. 3, the A(Si–H)/A(Si–CH_3) value gradually decreases with the increase of the $Fe(CO)_5$/AHPCS weight ratio.

According to our previous study in the AHPCS system [33–35], the consumption of Si–H bonds is due to the Si–Si dehydrocoupling (Eq. (2)) besides the hydrosilylation (Eq. (1)). In the present cross-linking of the AF precursors, the above FT IR results indicate that the consumption of Si–H bonds is simultaneously enhanced by the introduction of $Fe(CO)_5$.

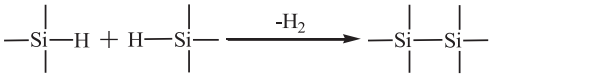

(2)

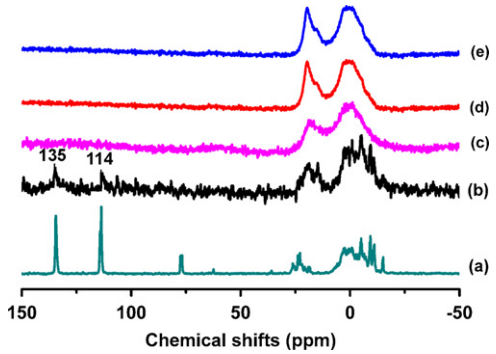

Fig. 1. ^{13}C NMR spectrum of the (a) soluble AHPCS (*$CDCl_3$ solvent) and solid-state ^{13}C MAS NMR spectra of cross-linked precursors: (b) AHPCS, (c) AF-1, (d) AF-2, and (e) AF-3.

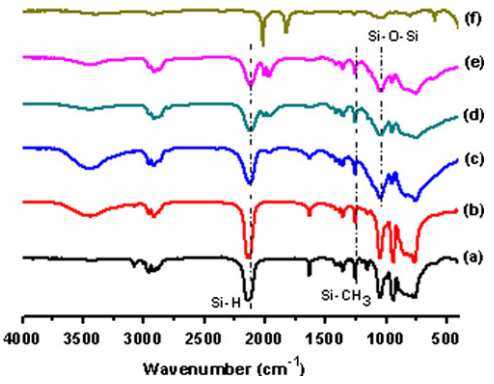

Fig. 2. FT IR spectra of (a) original AHPCS, (f) $Fe(CO)_5$ and cross-linked precursors: (b) AHPCS, (c) AF-1, (d) AF-2, and (e) AF-3.

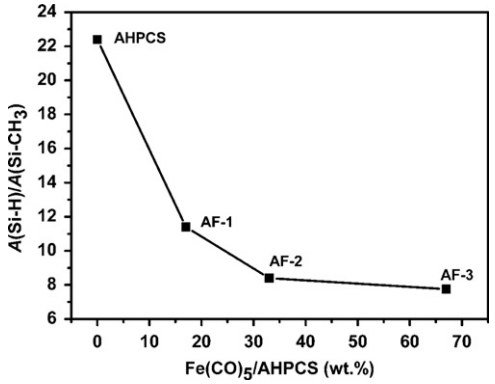

Fig. 3. Dependence of A(Si–H)/A(Si–CH_3) on $Fe(CO)_5$/AHPCS weight ratios.

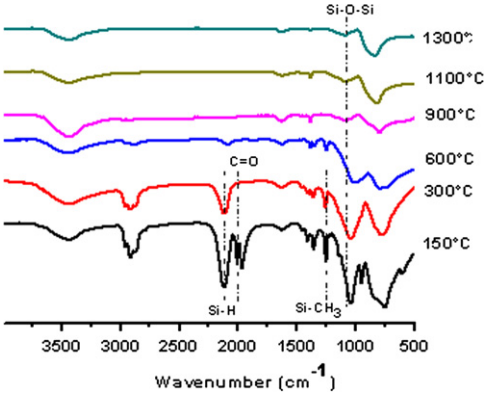

Fig. 4. FT IR spectra of AF-3 treated at different temperatures.

On the basis of the published literature [19], $Fe(CO)_5$ starts to decompose gradually into intermediate carbonyl derivatives. The carbonyl derivatives further react with one another to form carbonyls containing more iron nuclei, releasing CO gas [19]. It is thus believed that the evolved CO is then reacted with the Si–H bonds of AHPCS, forming the Si–O–Si linkage and rendering the cross-linking of AHPCS (Eq. (3)). This is confirmed by the fact of the appearance of stronger and broader peak at 1090 cm^{-1} (Si–O–Si stretch) with the increase of $Fe(CO)_5$/AHPCS weight ratio.

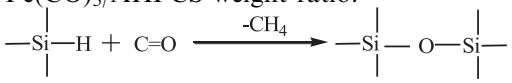

(3)

From the above analyses, it is believed that hydrosilylation, dehydrocoupling and the reaction of Si–H bonds with C═O groups evolved by $Fe(CO)_5$ decomposition are involved in the cross-linking of the AF precursors.

3.2. Ceramization

The structural changes during the ceramization of the AF precursors were analyzed by FT IR (Fig. 4). It is readily observed that the absorption of Si–H at 2140 cm^{-1} in AF-3 markedly decreases after heat treatment at 300 °C in comparison with that treated at 150 °C, which might be due to further cross-linking reaction of Si–H with Si–H (Eq. (2)) and/or Si–H with C═O (Eq. (3)). The peaks of C═O groups almost vanish, indicating that the decomposition of $Fe(CO)_5$ is completed. In the FT IR spectrum of the sample treated at 600 °C, the absorption of Si–CH_3 at 1250 cm^{-1} reduces when compared with that treated at 300 °C, which is attributed to the decomposition of organic side groups. Meanwhile, the intensity of Si–H at 2140 cm^{-1} almost disappears. At 900 °C, a broad band at around 800 cm^{-1} (attributed to SiC_4) and a small peak centered at 1090 cm^{-1} (attributed to Si–O–Si) are retained, while other bands at 1250 cm^{-1} (assigned to Si–CH_3) and 1040 cm^{-1} (from Si–CH_2–Si functionalities) are no longer observed in the FT IR spectrum. It is therefore believed that the conversion of polymer-to-ceramic is completed at around 900 °C. Further heating to 1100 and 1300 °C led to sharpening of the SiC band and shift from 780 to 850 cm^{-1} in position, which is consistent with the formation of crystalline SiC [36].

For macroscopic pyrolysis, the ceramic yields of the AFs at different temperatures were determined, with the results shown in Fig. 5. The ceramic yields of AF-1 and AF-2 are higher than that of AHPCS, while that of AF-3 is lower. It seems that the ceramic yield decreases with the increase of $Fe(CO)_5$ amount. The ceramic yield of AF-1 is the highest, which is 16 wt% higher than that of AHPCS. As indicated in Fig. 3, higher $Fe(CO)_5$/AHPCS weight ratio would lead to higher extent of cross-linking of the AF. However, the introduction of $Fe(CO)_5$ would be beneficial in enhancing the weight gain of the precursor because of the cross-linking, while at the same time readily lead to weight loss because of the decomposition of $Fe(CO)_5$. Therefore, the weight loss due to the decomposition of $Fe(CO)_5$ is dominative for AF-3, which has the highest $Fe(CO)_5$ content, leading to a lower ceramic yield in comparison with that of AHPCS.

As mentioned above, the ceramic yield of the precursor AF-1 is the highest. Therefore, the thermal behavior of the cross-linked AF-1 was investigated by TGA (Fig. 6). Careful examination of the TGA curve finds only 1% weight loss of AF-1 at 400 °C. As reported [37], the weight loss of PCS below 400 °C is predominately due to the evaporation of oligomers. Thus the above TGA results

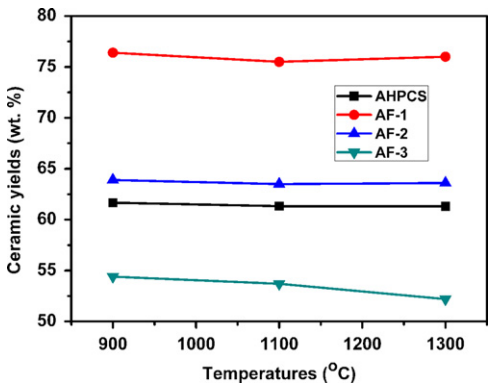

Fig. 5. Dependence of ceramic yields on $Fe(CO)_5$/AHPCS weight ratios.

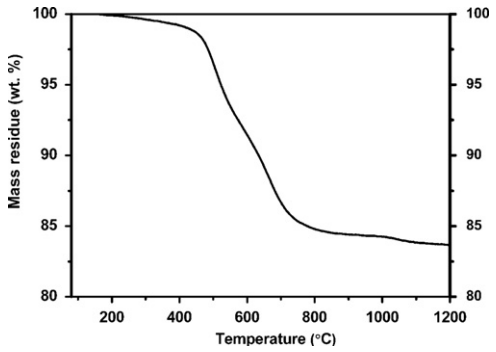

Fig. 6. TGA curve of cross-linked AF-1.

suggest that the low-molecular-weight oligomers in AF-1 were efficiently cross-linked by $Fe(CO)_5$ to prevent them from evaporation during heating. In the 400–900 °C region, the weight loss of AF-1 is 15%. It was well-known that above 300 °C, hydrogen (H_2) and methane (CH_4) are the major volatile species evolved during the pyrolysis of PCS, leading to the mass loss [38]. Generally speaking, the mass residue is constant at temperatures higher than 900 °C, that is, organic groups in AF-1 are completely decomposed below this temperature. The mass change is negligible in the temperature range of 900–1200 °C, indicating excellent heat-resistance of the obtained ceramic under argon gas. The TGA thermogram indicates a ceramic yield of 84% for the cross-linked AF-1 at 900 °C. However, the macroscopic pyrolysis experiment gives a lower yield of about 77% (Fig. 5), presumably because of the lower heating rate and the different heat history.

To analyze the ceramic composition, the EDS elemental analysis of the 1300 °C ceramics was measured and is shown in Fig. 7(a). The EDS spectrum exhibits characteristic peaks of silicon, iron, oxygen and carbon, confirming the ceramic composition. Evaluation of the EDS spectra indicates that the Fe content in the ceramic increases linearly with the increasing of the $Fe(CO)_5$/AHPCS weight ratio. Therefore, the Fe content in ceramics could be readily controlled by varying the $Fe(CO)_5$ content in the feed.

3.3. Microstructure of ceramics

The evolution of the crystalline phase was studied by XRD (Fig. 8). For the sample pyrolyzed at 600 °C, the product is amorphous and highly disordered. For the sample pyrolyzed at 900 °C, three peaks appear at $2\theta = 35.6°$, 60.0°, and 72.0°, corresponding to the (111), (220), and (311) lattice planes of β-SiC, respectively. The peaks become sharper with increase of the pyrolysis temperature, which is attributed to the increased degree of crystallization. A broad band appears at $2\theta = 45.2°$ in the XRD pattern of the sample pyrolyzed at 1100 °C, corresponding to the (110) plane of α-Fe [19].

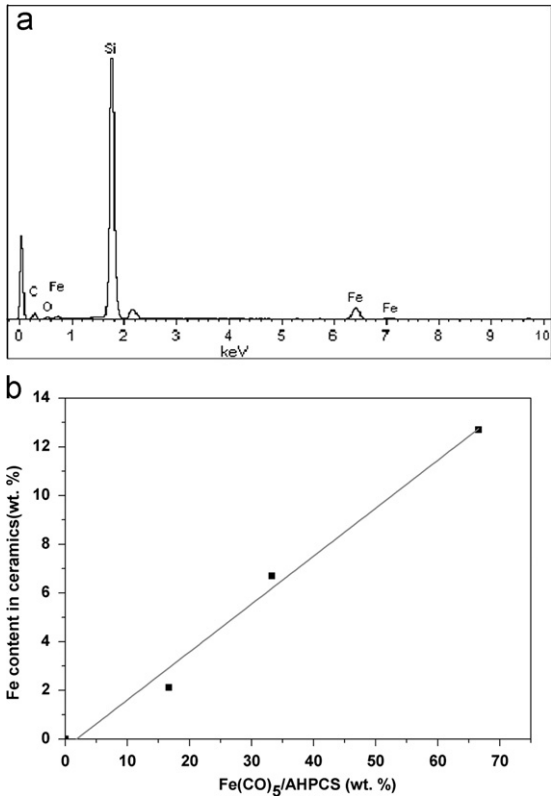

Fig. 7. (a) Typical EDS spectrum of AF-3-derived ceramic and (b) Fe content of SiFeC ceramic as a function of $Fe(CO)_5$/AHPCS weight ratios.

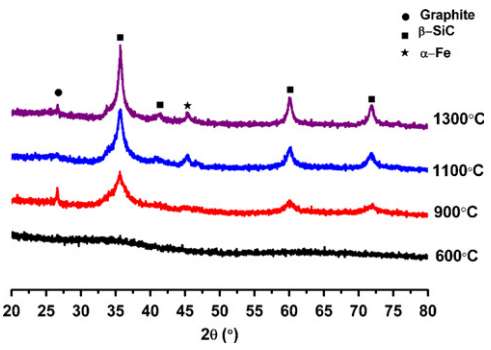

Fig. 8. XRD patterns of AF-3-derived ceramics at different temperatures.

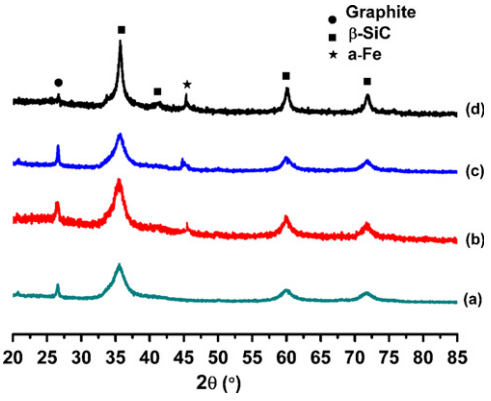

Fig. 9. XRD patterns of 1300 °C ceramics derived from (a) AHPCS, (b) AF-1, (c) AF-2 and (d) AF-3.

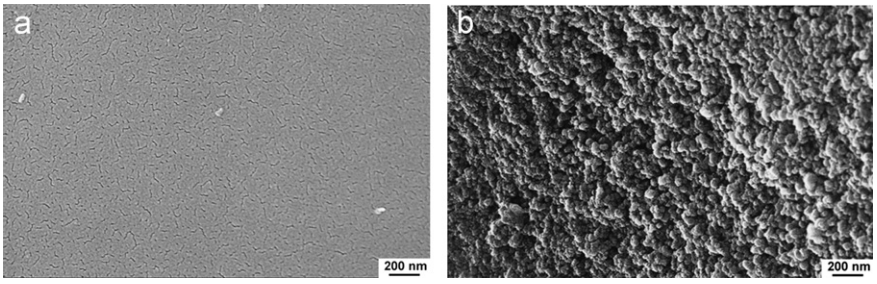

Fig. 10. SEM images of (a) AHPCS-derived ceramic and (b) AF-3-derived ceramic.

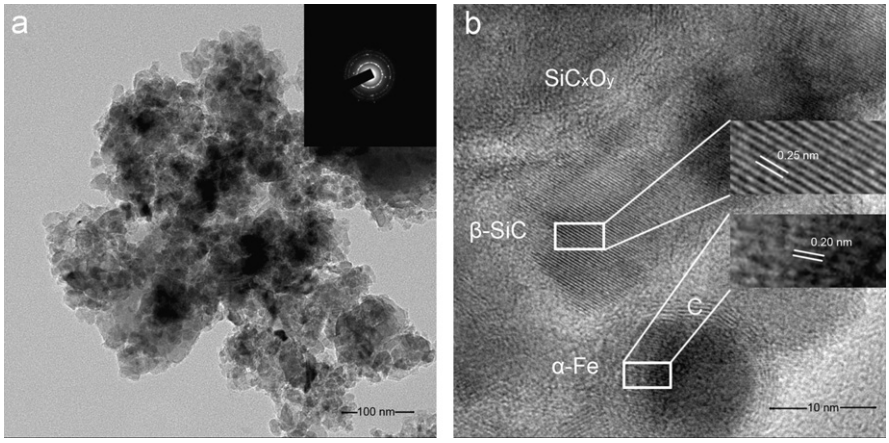

Fig. 11. (a) Bright field image and (b) HRTEM image of AF-3-derived ceramic.

In addition, the effect of $Fe(CO)_5$ content in feed on the crystallization behavior of the obtained ceramics pyrolyzed at 1300 °C was also investigated (Fig. 9). With increase of the $Fe(CO)_5$ content in the feed, the intensities of α-Fe peaks significantly increase, which matches very well with the increase of Fe content in the ceramics determined by EDS (Fig. 7(b)). Moreover, the growth of SiC crystals is improved by the introduction of iron into the ceramics. It has been reported [19] that the catalytic effect of iron on the decomposition of SiC_xO_y phase would lead to the growth of β-SiC crystals.

The microstructures of the 1300 °C ceramics derived from AHPCS and AF-3 were investigated by SEM, and the results are shown in Fig. 10. It is evident that the crystal particle of AF-3-derived SiFeC ceramic is larger than that of the AHPCS-derived SiC ceramic, indicating that the Fe-containing SiC would be much better crystallized than SiC. The results agree well with the XRD patterns.

To further investigate the iron morphology in the SiFeC ceramic, TEM observations were performed, and the results are shown in Fig. 11. Fig. 11(a) demonstrates that the AF-3-derived ceramic annealed at 1300 °C consists of SiC and Fe nano-crystals with grain size in the range of 10–20 nm. Fig. 11(b) shows that α-Fe crystallites of 10 nm, together with β-SiC crystallites of about 15 nm and poorly organized turbostratic carbon, are dispersed in an amorphous SiC_xO_y matrix, indicating a microstructure of Fe-containing SiC ceramic nanocomposites. It is believed that the decomposition of $Fe(CO)_5$ leads to formation of α-Fe in the ceramic nanocomposites.

3.4. Magnetic properties of ceramics

Fig. 12 shows the magnetization curves for the 1300 °C ceramics derived from AF precursors. It is found that all of the ceramics are magnetizable (Fig. 12(a)). Their magnetization increases rapidly with the increase of the applied field strength and becomes constant over the field strength of 3000 Oe. The three samples exhibit some hysteresis loops. For AF-3-derived ceramic, the highest remnant magnetization Mr and coercivity Hc are 0.4 emu/g and 125 Oe, respectively. The results suggest that the ceramics are basically soft magnetic materials. In addition, the saturation magnetization (Ms) of the ceramics increases with the increase of $Fe(CO)_5$/AHPCS ratio in the feeds, which is thought to be caused by the increasing content of α-Fe in the final SiFeC ceramic (Fig. 12(b)).

4. Conclusions

In this paper, Fe-containing SiC ceramic nanocomposites were prepared by the PDC route, using AHPCS-$Fe(CO)_5$ precursors as starting materials. On one hand, $Fe(CO)_5$ was used as a new source of Fe in the final ceramic nanocomposites. On the other hand, the cross-linking

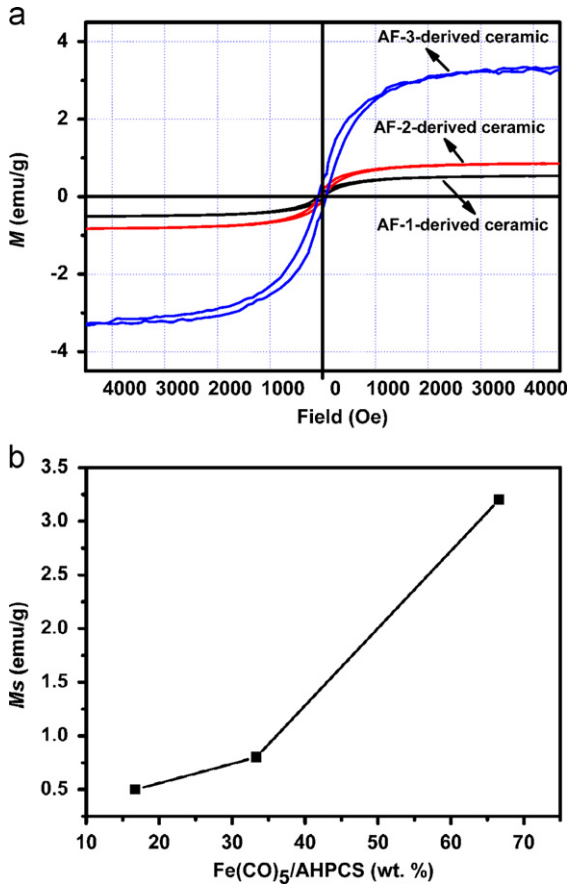

Fig. 12. (a) Magnetization versus field measurements for AF-derived ceramics and (b) dependence of Ms on $Fe(CO)_5$/AHPCS weight ratios.

of AHPCS involving hydrosilylation reactions had been improved by $Fe(CO)_5$, which acted as an effective catalyst during hydrosilylation cross-linking. The ceramic yield of AF-1 is 16 wt% higher than that of AHPCS. However, the ceramic yield decreases with increase of $Fe(CO)_5$ in the feed, which is attributed to the dominative weight loss of the decomposition of $Fe(CO)_5$ compared with the weight gain of the cross-linking of AF by $Fe(CO)_5$ during ceramization. Both the increase of pyrolysis temperature and the introduction of Fe have been found to improve the degree of crystallization of the final ceramic. The TEM observation suggests that α-Fe crystallites and β-SiC crystallites, together with poorly organized turbostratic carbon, are dispersed in an amorphous SiC_xO_y matrix. This type of microstructure might be responsible for the soft magnetization of the obtained ceramic nanocomposites. The iron content and the magnetic properties of the final ceramic could be easily controlled by adjusting the amount of $Fe(CO)_5$ in the precursor.

Acknowledgments

This work is supported by the Natural Science Foundation of China (NSFC) (No. 50802079) and the Natural Science Foundation of Fujian Province of China (No. 2011J01330).

References

[1] X. Liu, M.C. Zheng, K. Xie, Mechanism of lithium storage in Si–O–C composite anodes, Journal of Power Sources 196 (2011) 10667–10672.
[2] J.H. Shin, B.V.M. Kumar, J.H. Kim, S.H. Hong, Tribological properties of Si_3N_4/SiC nano–nano composite ceramics, Journal of the American Ceramic Society 94 (2011) 3683–3685.
[3] R.S. Kumar, D. Sivakumar, K. Venkateswarlu, A.S. Gandhi, Mechanical behavior of molybdenum disilicide reinforced silicon carbide composites, Scripta Materialia 65 (2011) 838–841.
[4] P. Colombo, G. Mera, R. Riedel, G.D. Soraru, Polymer-derived ceramics: 40 years of research and innovation in advanced ceramics, Journal of the American Ceramic Society 93 (2010) 1805–1837.
[5] E. Ionescu, H.J. Kleebe, R. Riedel, Silicon-containing polymer-derived ceramic nanocomposites (PDC-NCs): preparative approaches and properties, Chemical Society Reviews 41 (2012) 5032–5052.
[6] M.J. Maclachlan, M. Ginzburg, N. Coombs, T.W. Coyle, N.P. Raju, J.E. Greedan, G.A. Ozin, I. Manners, Shaped ceramics with tunable magnetic properties from metal-containing polymers, Science 287 (2000) 1460–1463.
[7] I. Manners, Putting metals into polymers, Science 294 (2001) 1664–1666.
[8] A. Francis, E. Ionescu, C. Fasel, R. Riedel, Crystallization behavior and controlling mechanism of iron-containing Si–C–N ceramics, Inorganic Chemistry 48 (2009) 10078–10083.
[9] Y. Li, Z. Zheng, C. Reng, Z. Zhang, W. Gao, S. Yang, Z. Xie, Preparation of Si–C–N–Fe magnetic ceramics from iron-containing polysilazane, Applied Organometallic Chemistry 17 (2003) 120–126.
[10] R. Hauser, A. Francis, R. Theismann, R. Riedel, Processing and magnetic properties of metal-containing SiCN ceramic micro- and nano-composites, Journal of Materials Science 43 (2008) 4042–4049.
[11] J.P. Li, Z.J. Zhang, Z.M. Zheng, L. Guo, G.Y. Xu, Z.M. Xie, Preparation and magnetic properties of Fe/Si/C/N ceramics derived from a polymeric precursor, Journal of Applied Polymer Science 105 (2007) 1786–1792.
[12] Q. Li, X.W. Yin, L.Y. Feng, Dielectric properties of Si_3N_4–SiCN composite ceramics in X-band, Ceramics International 38 (2012) 6015–6020.
[13] X.W. Yin, Y.Y. Xue, L.T. Zhang, L.F. Cheng, Dielectirc, electromagnetic absorption and interference shielding properties of porous yttria-stabilized zirconia/silicon carbide composites, Ceramics International 38 (2012) 2421–2427.
[14] X.M. Li, L.T. Zhang, X.W. Yin, Z.J. Yu, Mechanical and dielectric properties of porous Si_3N_4–SiC(BN) ceramic, Journal of Alloys and Compounds 490 (2010) L40–L43.
[15] F. Ye, L.T. Zhang, X.W. Yin, X.Z. Zuo, Y.S. Liu, L.F. Cheng, Fabrication of Si_3N_4–SiBC composite ceramic and its excellent electromagnetic properties, Journal of the European Ceramic Society 32 (2012) 4025–4029.
[16] Q.H. Sun, J.W.Y. Lam, K.T. Xu, H.Y. Xu, J.A.K. Cha, P.C.L. Wong, G.H. Wen, X.X. Zhang, X.B. Jing, F.S. Wang, B.Z. Tang, Nanocluster-containing mesoporous magnetoceramics from hyperbranched organometallic polymer precursors, Chemistry of Materials 12 (2000) 2617–2624.
[17] Q.H. Sun, K.T. Xu, H. Peng, R.H. Zheng, M. Haussler, B.Z. Tang, Hyperbranched organometallic polymers: synthesis and properties of poly(ferrocenylenesilyne)s, Macromolecules 36 (2003) 2309–2320.
[18] Z.Y. Chen, X.D. Li, J. Wang, W.F. Li, Preparation of continuous Si–Fe–C–O functional ceramic fibers, Transactions of Nonferrous Metals Society of China 17 (2007) 987–991.
[19] X. Chen, Z. Su, L. Zhang, M. Tang, Y. Yu, L. Zhang, L. Chen, Iron nanoparticle-containing silicon carbide fibers prepared by pyrolysis

of $Fe(CO)_5$-doped polycarbosilane fibers, Journal of the American Ceramic Society 93 (2010) 89–95.
[20] L.V. Interrante, Q.H. Shen, in: R.G. Jones et al. (Ed.), Silicon Containing Polymers, Kluwer Academic Publishers, Dordrecht, 2000, pp. 247–321.
[21] L.V. Interrante, Q.H. Shen, Hyperbranched polycarbosilanes via nucleophilic substitution reactions, in: P.R. Dvornic, M.J. Owen (Eds.), Silicon-Containing Dendritic Polymers, Springer Science and Business Media B.V., Dordrecht, 2009, pp. 315–343.
[22] T.H. Huang, Z.J. Yu, X.M. He, M.H. Huang, L.F. Chen, H.P. Xia, L.T. Zhang, One-pot synthesis and characterization of a new, branched polycarbosilane bearing allyl groups, Chinese Chemical Letters 18 (2007) 754–757.
[23] M.H. Huang, Y.H. Fang, R. Li, Z.J. Yu, H.P. Xia, Synthesis and properties of liquid polycarbosilanes with hyperbranched structures, Journal of Applied Polymer Science 113 (2009) 1611–1618.
[24] Y.H. Fang, M.H. Huang, Z.J. Yu, H.P. Xia, L.F. Chen, Y. Zhang, L.T. Zhang, Synthesis, characterization and pyrolytic conversion of a novel liquid polycarbosilane, Journal of the American Ceramic Society 91 (2008) 3298–3302.
[25] Z.J. Yu, R. Li, J.Y. Zhan, C. Zhou, L. Yang, G.M. He, H.P. Xia, Synthesis and characterization of a propargyl-substituted polycarbosilane with high ceramic yield, Journal of Applied Polymer Science 121 (2011) 3400–3406.
[26] Z.J. Yu, M.H. Huang, R. Li, J.Y. Zhan, G.M. He, H.P. Xia, Studies on cross-linking of a liquid polycarbosilane initiated by 2,2′-azobisisobutyronitrile, Journal of the Chinese Ceramic Society 37 (2009) 1373–1377.
[27] Z.J. Yu, M.H. Huang, R. Li, J.Y. Zhan, G.M. He, M.T. Ding, H.P. Xia, Application of dibenzoyl peroxide in cross-linking of a liquid polycarbosilane, Journal of Functional Materials 40 (2009) 2058–2060.
[28] J. Yu, J.Y. Zhan, M.H. Huang, R. Li, C. Zhou, G.M. He, H.P. Xia, Preparation of a hyperbranched polycarbosilane precursor to SiC ceramics following an efficient room-temperature cross-linking process, Journal of Materials Science 45 (2010) 6151–6158.
[29] Z.J. Yu, J.Y. Zhan, C. Zhou, L. Yang, R. Li, H.P. Xia, Synthesis and characterization of SiC(Ti) ceramics derived from a hybrid precursor of titanium-containing polycarbosilane, Journal of Inorganic and Organometallic Polymers and Materials 21 (2011) 412–420.
[30] E. Lukevics, Z.V. Belyakova, M.G. Pometantseva, Organometallic chemistry reviews, in: D. Seyferth, A.J. Davies, E.O. Fischer (Eds.), Journal of Organometallic Chemistry Library, 5, Elsevier, Amsterdam, 1977, pp. 1–181.
[31] G.F. Huang, S.B. Li, Z.G. Sun, S.Q. Huang, Advance of catalyst on hydrosilylation reaction, Journal of Molecular Catalysis (China) 14 (2000) 409–418.
[32] D.F. Shriver, M.A. Drezdzon, The Manipulation of Air-Sensitive Compounds, 2nd ed., Wiley, New York, 1986.
[33] H.B. Li, L.T. Zhang, Y.G. Wang, Z.J. Yu, M.H. Huang, H.B. Tu, H.P. Xia, Polymer–ceramic conversion of liquid polycarbosilane for SiC-based ceramics, Journal of Materials Science 43 (2008) 2806–2811.
[34] H.B. Li, L.T. Zhang, Y.G. Wang, Z.J. Yu, M.H. Huang, H.B. Tu, H.P. Xia, Effect of the polycarbosilane structure on its final ceramic yield, Journal of the European Ceramic Society 28 (2008) 887–891.
[35] Z.J. Yu, L. Yang, J.Y. Zhan, C. Zhou, H. Min, Q. Zheng, H.P. Xia, Preparation, cross-linking and ceramization of AHPCS/Cp_2ZrCl_2 hybrid precursors for SiC/ZrC/C composites, Journal of the European Ceramic Society 32 (2012) 1291–1298.
[36] G. Ramis, P. Quintard, M. Gauchetier, G. Busca, V. Lorenzelli, Surface chemistry and structure of ultrafine silicon carbide: an FT-IR study, Journal of the American Ceramic Society 72 (1989) 1692–1697.
[37] Q. Liu, H.J. Wu, R. Lewis, G.E. Maciel, L.V. Interrante, Investigation of the pyrolytic conversion of poly(silylenemethylene)to silicon carbide, Chemistry of Materials 11 (1999) 2038–2048.
[38] M. Takeda, A. Saeki, J. Sakamoto, Y. Imai, H. Ichikawa, Effect of hydrogen atmosphere on pyrolysis of cured polycarbosilane fibers, Journal of the American Ceramic Society 83 (2000) 1063–1069.